Original Article

http://www.jcpjournal.org
pISSN 2288-3649 · eISSN 2288-3657
https://doi.org/10.15430/JCP.2022.27.2.112

JCP

Formoxanthone C Inhibits Malignant Tumor Phenotypes of Human A549 Multidrug Resistant-cancer Cells through Signal Transducer and Activator of Transcription 1-Histone Deacetylase 4 Signaling

Chutima Kaewpiboon[1,*], Nawong Boonnak[2], Sirichat Kaowinn[3], Natpaphan Yawut[4], Young-Hwa Chung[4,*]

[1]Department of Biology, Faculty of Science, Thaksin University, Phatthalung, [2]Department of Basic Science and Mathematics, Faculty of Science, Thaksin University, Songkhla, [3]Department of General Science and Liberal Arts, King Mongkut's Institute of Technology Ladkrabang Prince of Chumphon Campus, Chumphon, Thailand, [4]Department of Cogno-Mechatronics Engineering, Pusan National University, Busan, Korea

Considering that presence of cancer stem cell (CSC) subpopulation in tumor tissues confers anticancer drug resistance, we investigated whether human A549 lung cancer cells resistant to etoposide possess CSC-like phenotypes. Furthermore, it is known that these malignant tumor features are the leading cause of treatment failure in cancer. We have thus attempted to explore new therapeutic agents from natural products targeting these malignancies. We found that formoxanthone C (XanX), a 1,3,5,6-tetraoxygenated xanthone from *Cratoxylum formosum* ssp. *pruniflorum*, at a non-cytotoxic concentration reduced the expression of the signal transducer and activator of transcription 1 (STAT1) and histone deacetylase 4 (HDAC4) proteins, leading to inhibition of CSC-like phenotypes such as cell migration, invasion, and sphere-forming ability. Moreover, we found that treatment with STAT1 or HDAC4 small interfering RNAs significantly hindered these CSC-like phenotypes, indicating that STAT1 and HDAC4 play a role in the malignant tumor features. Taken together, our findings suggest that XanX may be a potential new therapeutic agent targeting malignant lung tumors.

Key Words Formoxanthone C, Multidrug resistant-cancer, Cancer stem cell-like phenotypes, Signal transducer and activator of transcription 1, Histone deacetylase 4

INTRODUCTION

Lung cancer represents the most common malignancy and is responsible for the leading cause of cancer-related mortality and death worldwide [1]. Unfortunately, the success of chemotherapy is hindered by the development of multidrug resistance (MDR) in cancer. The increase of drug efflux out of cells mediated by P-glycoprotein (P-gp) is a main mechanism on drug resistance in cancer cells [2]. Furthermore, cancer cells resistant to chemotherapy treatment usually demonstrate aggressive characteristics, such as accelerated metastasis to distant organs or tissues and self-renewal into multiple cell types [3]. Recent studies have shown up-regulation of P-gp mediated by signal transducer and activator of transcription 1 (STAT1)-histone deacetylase 4 (HDAC4) in the etoposide-resistant human lung cancer cell line (A549RT-eto) [4].

STAT1 is one of the seven mammalian members of the STAT family and a master transcription factor for IFN-γ intracellular signaling, leading to anti-oncogenesis in part by upregulating caspases [5], cyclin-dependent kinase inhibitor 1A [6], and the IFN-regulatory Factor 1 (IRF1)/p53 pathway [7], while down-regulating the BCL2 family [8]. Recent reports have also shown that constitutive overexpression of STAT1 is correlated with protection of tumor cells from chemotherapeutic drugs such as doxorubicin [9] or cisplatin [10]. Furthermore, other studies demonstrated that STAT1 promotes the

Received April 21, 2022, Revised June 9, 2022, Accepted June 9, 2022
Correspondence to Chutima Kaewpiboon, E-mail: Chutima.k@tsu.ac, https://orcid.org/0000-0003-2519-3796
Young-Hwa Chung, E-mail: younghc@pusan.ac.kr, https://orcid.org/0000-0001-5738-7400
*These authors contributed equally to this work as co-correspondence authors.

epithelial-mesenchymal transition (EMT) and manifestation of cancer stem cell (CSC)-like phenotypes such as faster cell migration, aggressive invasion and enhanced sphere-forming ability [11,12].

Histone deacetylases (HDACs) play roles in the maintenance and function of chromatin by regulating the acetylation state of histones [13]. However, recent studies suggest that HDACs also regulate the acetylation state of many non-histone targets [14-16]. Notably, HDAC4 downregulation inhibits EMT and reduces the characteristics of CSC [17]. Furthermore, STAT1-HDAC4 signaling induced by EMT [18] and doxorubicin resistance in human lung cancer cells overexpressing cancer upregulated gene 2 [19].

Novel therapeutic agents from natural products against anti-cancer drug resistance becomes the major challenge in cancer therapies. Natural products from plants have been a rich source of chemotherapeutic agents [20]. One of them is formoxanthone C (XanX), a xanthone from the green fruit of *Cratoxylum formosum* ssp. *pruniflorum* [21]. This xanthone has exhibited cytotoxic activities against the NCI-H187 and human small-cell lung cancer cell lines [22,23]. Moreover, XanX reverses etoposide resistance in A549RT-eto cells by induction of both autophagy and apoptosis, and confers cytotoxicity through down-regulation of HDAC4 [4].

This study was initiated to investigate whether A549RT-eto cancer cells harbor other CSC-like phenotypes in addition to drug resistance and whether the STAT1-HDAC4 signaling pathway is involved in the manifestation of such additional phenotypes. Furthermore, we explored whether formoxanthone C (XanX) could effectively inhibit the malignant phenotypes through suppression of STAT1-HDAC4 in A549RT-eto cells.

MATERIALS AND METHODS

Plant material

Green fruits of the *C. formosum* ssp. *pruniflorum* were collected in August 2008 from Pha Yao Province, in the northern part of Thailand. A voucher specimen (No. 0012677) has been deposited at the Prince of Songkla University Herbarium [21].

Preparation of XanX

Air-dried green fruits of *C. formosum* ssp. *pruniflorum* were successively extracted with dichloromethane (CH_2Cl_2) to yield the crude extract of CH_2Cl_2 which was further subjected to quick column chromatography and followed by column chromatography on silica gel to yield XanX. The purity of XanX was examined using ^{1}H NMR as described previously [22].

Cell cultures

Human lung cancer A549 cells (ATCC, Manassas, VA, USA) and A549RT-eto cells, which were developed and generously provided by the Laboratory of Biochemistry, Chulabhorn Research Institute, Thailand, as described elsewhere [24]. The cells were cultured in RPMI-1640 medium (Gibco, Grand Island, NY, USA), supplemented with 10% FBS, 1% penicillin, and streptomycin (Gibco), at 37°C in a humidified atmosphere of 5% carbon dioxide in air.

Cell viability assay

The cells were plated into 24 well plates at (1×10^5 cells per well) for overnight to achieve 80% to 90% confluency before XanX treatment. Then, 3-(4,5-dimethylthiazol-2-yl)-2,5-diphenyltetrazolium bromide (MTT) assay (CellTiter 96 Non-Radioactive Cell Proliferation assay; Promega Corporation, Madison, WI, USA) was used to measure cell survival, as previously described [25]. Dye solutions containing tetrazolium were added to the cells in the 24-well plate and incubated for 2 hours. The absorbance of the formazan produced by living cells was measured at a wavelength of 570 nm (Victor3; PerkinElmer, Waltham, MA, USA). The relative percentage of cell survival was calculated by the mean optical density of treated cells (ODT) and the mean optical density of control cells (ODC) with the following formula: Cell survival rate = (ODT/ODC).

Antibodies

For immunoblotting, antibodies against STAT1 (#9172) and phospho-STAT1 (#9171) were acquired from Cell Signaling Biotechnology (Beverly, MA, USA). Anti-P-gp (Calbiochem, San Diego, CA, USA) and anti-actin (C4), -Klf4 (sc-166229), -HDAC4 (sc-5245) antibodies were purchased from Santa Cruz Biotechnology (Santa Cruz, CA, USA). Anti-E-cadherin (ab15148), -N-cadherin (ab18203), -Vimentin (ab137321), -Bmi1 (ab126783), -Sox2 (ab97959), -Nanog (ab80892) and -Oct4 (ab109183) were obtained from Abcam (Cambridge, MA, USA).

Immunoblotting

The cells were harvested and lysed with lysis buffer (150 mM NaCl, 1% NP-40, 50 mM Tris-HCl [pH 7.5] containing 0.1 mM Na_2VO_3, 1 mM NaF, and protease inhibitors [Sigma Aldrich, St. Louis, MO, USA]). For immunoblotting, proteins from whole-cell lysates were resolved by 10% sodium dodecyl sulfate (SDS)-polyacrylamide gel electrophoresis (PAGE) and then transferred to nitrocellulose membranes. After that the membranes were incubated with PBS containing 0.05% Tween 20 and 5% skimmed milk for 1.5 hours at room temperature. After washing, the membranes incubated separately with primary antibodies (1:1,000 or 1:2,000 dilution) for overnight at 4°C. After washing, the membranes were incubated with the secondary antibodies (1:2,000 dilution), horseradish peroxidase–conjugated rabbit anti-goat or mouse Immunoglobulin G, at room temperature. Immunodetection was performed using chemiluminescence reagent and exposed for an enhanced chemiluminescence assay using LAS 4000 mini (GE Healthcare, Durham, NC, USA). Densitometric analysis

of protein bands from all experiments were performed using ImageJ software (https://imagej.nih.gov/ij/) for image analysis [26]. The visualization of β-actin was used to ensure equal sample loading in each lane. All experiments were repeated at least 3 times.

Immunofluorescence

The cells were fixed with 4% paraformaldehyde for 15 minutes, permeabilized with cold ethanol for 15 minutes, blocked with 10% bovine serum albumin for 30 minutes, and treated with primary antibodies (1:100 dilution) for 30 minutes at room temperature. After incubation, the cells were washed three times with PBS, incubated with Alexa Fluor 418-conjugated goat anti-mouse or donkey anti-rabbit antibody (1:500 dilution; Molecular Probes, Eugene, OR, USA) in PBS for 30 minutes. at room temperature, and washed three times with PBS. For nuclear staining, the cells were incubated with 4′, 6-diamidino-2-phenylindole (DAPI) for 5-10 minutes in the dark and washed three times with PBS. The stained cells were mounted using PBS containing 10% glycerol and photographed using a fluorescence microscope (Axio Observer D1; Zeiss, Oberkochen, Germany).

Small interference RNA transfection

The cells were plated into 24 well plates at (1×10^5 cells per well) for overnight to achieve 60% to 70% confluency before small interfering RNA (siRNA) transfection as previously described [18], Human STAT1-siRNAs (100 nM ; Bioneer, Daejeon, Korea), human HDAC4-siRNAs (100 nM; Bioneer), or negative control siRNAs (100 nM; Bioneer) were mixed with Lipofectamine 2000 (Invitrogen). The cells were incubated with the transfection mixture for 24 hours and then rinsed with RPMI-1640 medium containing 10% FBS. The cells were incubated for 24 hours before harvest.

Sphere formation assay

As described previously [18], the cells were cultured in tumor sphere medium consisting of serum-free DMEM/F12 medium (Gibco), 20 ng/mL human recombinant epidermal growth factor (EGF) (Invitrogen), 10 ng/mL basic fibroblast growth factor (Invitrogen), 5 g/mL insulin (Sigma Aldrich, St. Louis, MO, USA) and 0.4% bovine serum albumin (Sigma Aldrich), then cells at density of 1,000 cells/well suspended in sphere medium with or without XanX were plated in 24-well ultra-low attachment plates. Two, four or six day later, tumor sphere formation was visualized and photographed under a microscope. The size and the number of spheroids were analyzed under a light microscope. Spheroids more than 50 μm in size served as a criterion for sphere formation.

Wound-healing assay

The cells (1×10^5 cells/well) were plated in growth medium in 24-well plates and incubated for 24 hours. After confirming the formation of a complete monolayer almost 100%, the cells were wounded by scratching lines with a standard 200-μL plastic tip as described previously [18]. The wound was generated and then the cells were washed with PBS. The medium with or without XanX was added the cells and incubated for 24 hours. Migration and cell movement throughout the wound area were visualized and photographed under a phase-contrast microscope at 0 and 24 hours. The cell wound closure rate was calculated using the following equation: Wound closure = [1-(wound area at Tt/wound area at T0)] × 100, where Tt is the time passed since wounding and T0 is the time the wound was created. The experiments were performed in triplicate.

Transwell invasion assay

The cell invasive capacity was measured using Transwell Filter (8-μm pore size; Corning, Corning, NY, USA) with Matrigel (BD Biosciences, San Jose, CA, USA). The cells treated with XanX or untreated at density of 5×10^4 cells/well were transferred to each upper chamber of Transwell in 200 μL of serum-free medium. As mentioned elsewhere [18], 500 μL of complete medium was added to each bottom chamber of Tranwell with the same concentration of XanX. After incubation for 24 hours, the cells in the upper chambers were removed, and the invading cells in the membrane were stained with hematoxylin-eosin. The stained cells were photographed and counted under a light microscope in at least six randomly selected fields.

Statistical analysis

Data are expressed as the mean ± standard error of the mean (SEM). Statistical analysis involved calculating the unpaired t-test using GraphPad InStat (GraphPad Software, San Diego, CA, USA). Values significantly different from the control are shown at $^*P < 0.05$, $^{**}P < 0.01$, and $^{***}P < 0.001$.

RESULTS

A549RT-eto cells exhibit faster cell migration and more aggressive invasion than the control cells

Since we observed that human A549RT-eto exhibit upregulation of STAT1 and HDAC4 and the elevated levels of P-gp encoded by *MDR* [4], we next explored whether A549RT-eto cells contribute to other malignant tumor features such as cell migration and invasion. Cell migration was observed after the center of the monolayers of A549RT-eto and their parental cells were scratched. A549RT-eto cells demonstrated higher cell migration rates compared to those of A549 cells (Fig. 1A) ($^{***}P < 0.001$, A549RT-eto vs. the A549 cell). In addition, both cell lines were cultured in the upper chamber of transwell coated with Matrigel (Sigma Aldrich). The number of A549RT-eto invading cells in the lower chamber of transwell was significantly higher than that of A549 cells (approximately two-fold) after staining with hematoxylin-eosin (Fig. 1B). More-

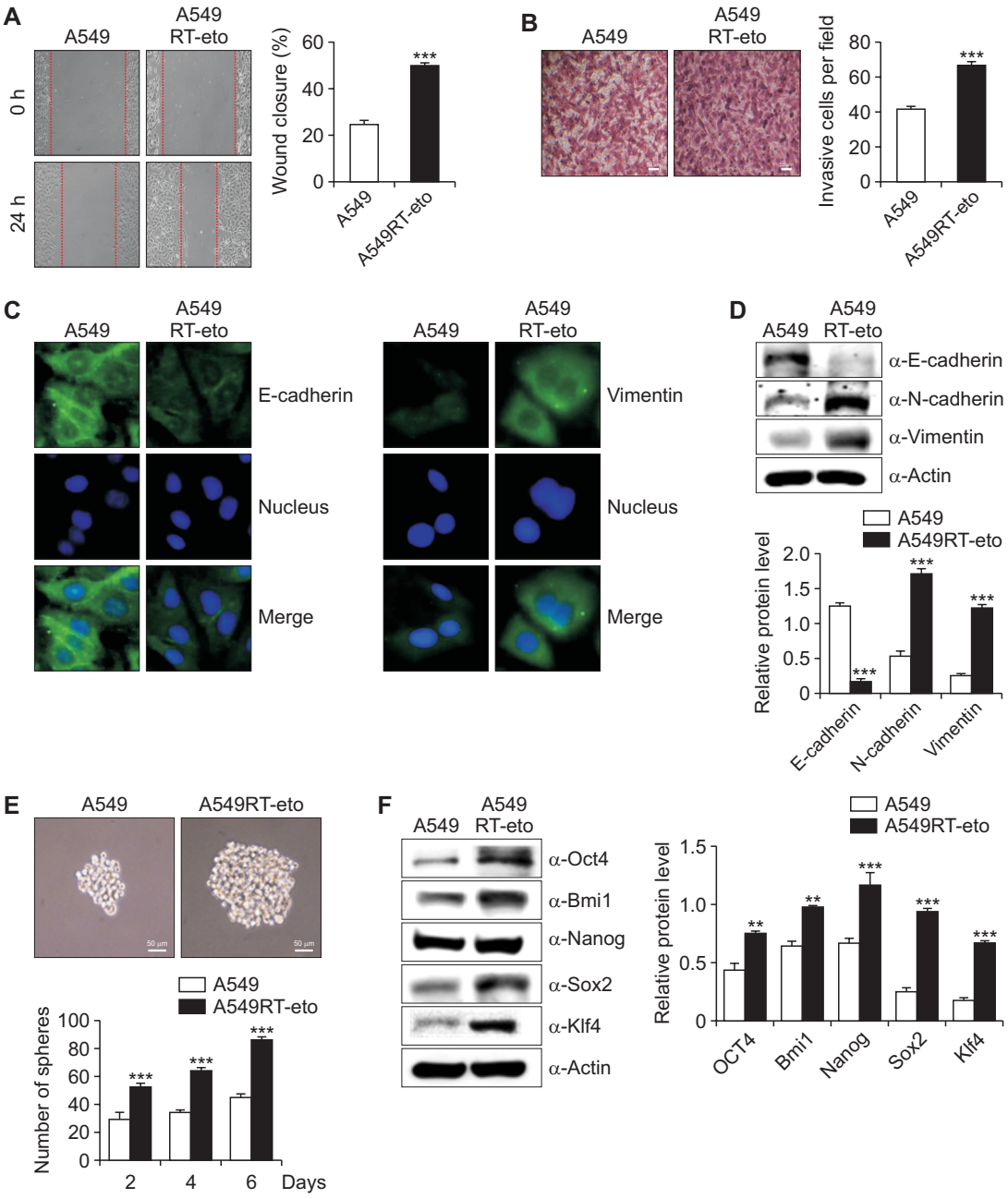

Figure 1. A549RT-eto cells exhibit CSC-like phenotypes. (A) Cell migration was measured by a wound-healing assay after treatment for 24 hours. The cell wound closure rate was measured at 24 hours and was calculated according to the equation described in Materials and Methods. The experiments were performed in triplicate (***P < 0.001, A549RT-eto vs. the A549 cell). (B) An invasion assay was performed using 24-well chambers coated with Matrigel after 24 hours. The invading cells in the membrane were stained with hematoxylin-eosin. (C) The expression of E-cadherin and vimentin was detected by immunofluorescence using an Alexa Fluor 488-conjugated secondary antibody (green; outside part). DAPI was added for nuclear staining (blue; inside part) (magnificaiton ×400). (D) Lysates from A549 and A549RT-eto cells were prepared and separated on an 8% SDS-PAGE gel. The expression of E-cadherin, N-cadherin and vimentin was detected by immunoblotting. Densitometric analysis was performed on all blots and the integrated optical density of each band was normalized with corresponding β-actin (***P < 0.001, A549RT-eto vs. the A549 cells). (E) The spheroid size and the number of A549 and A549RT-eto cells were evaluated after 2, 4 and 6 days. A spheroid greater than 50 μm in size was counted as the criterion for evaluating sphere formation. Scale bars indicate 50 μm. The assay was carried out from three independent experiments (***P < 0.001, A549RT-eto vs. A549 cells). (F) The expressions of Oct4, Bmi1, Nanog, Sox2 and Klf4 was detected by immunoblotting after 24 hours. Densitometric analysis was performed on all blots and the integrated optical density of each band was normalized with corresponding β-actin (**P < 0.05 and ***P < 0.001, A549RT-eto vs. the A549 cells). A549RT-eto, A549 lung cancer cells resistant to etoposide; CSC, cancer stem cell; DAPI, diamidino-2-phenylindole; SDS, sodium dodecyl sulfate; PAGE, polyacrylamide gel electrophoresis.

over, A549RT-eto cells lost the expression of proteins that promote cell–cell contact such as E-cadherin, and gained the expression of mesenchymal markers such as vimentin and N-cadherin, as well as protein markers of EMT (Fig. 1C) (***P < 0.001, A549RT-eto vs. the A549 cells). Subsequently, immunofluorescence microscopy confirmed that A549RT-eto cells show decreased E-cadherin staining and increased vimentin staining unlike A549 cells (Fig. 1D). These results suggest that A549RT-eto as MDR cancer cells exhibit faster cell migration and more aggressive cell invasion compared to those of the parental A549 cells.

A549RT-eto cells exhibit increased stemness-related factor expression and sphere formation

CSCs play a major role in cancer initiation, progression, metastasis, and drug resistance [27] CSC-like features include sphere formation and elevated expression of stemness-related factors such as Sox2, Oct4, Klf4, Bmi1 and Nanog. We thus exploered whether A549RT-eto cells could exhibit CSC-like phenotypes. Because the sphere formation assay is considered a useful method to evaluate self-renewal of CSCs in vitro [28], we compared the sphere-forming ability of A549RT-eto cells with that of the parental cells. A549RT-eto cells exhibited a larger size and the greater number of spheroids compared to those of their parental cells (Fig. 1E) (***P < 0.001, A549RT-eto vs. A549 cells). In addition, A549RT-eto cells had enhanced protein expression of the stemness-related factors (Fig. 1F) (**P < 0.05 and ***P < 0.001, A549RT-eto vs. the A549 cells). Therefore, these results suggest that A549RT-eto cells exhibit CSC-like phenotypes.

XanX suppresses the expression of STAT1, HDAC4, and P-gp in A549RT-eto cells

A549RT-eto cells were shown to exhibit enhanced P-gp protein levels, which lead to MDR through upregulation of the STAT1-HDAC4 signaling [4]. Thus, we screened natural compounds derived from medicinal plants in Thailand to reverse MDR via suppression of the STAT1-HDAC4 signaling. The compound isolated from *Cratoxylum formosum* ssp. *pruniflorum* was characterized as XanX [22]. The molecular structure of XanX is shown in Figure 2A. Previously, we have reported that XanX efficiently induces A549RT-eto cell death at the concentration of 20 μg/mL [4]. Next, we further optimized the non-toxic concentration of XanX at 10 μg/mL for 24 hours. We found that A549RT-eto cells were still alive in the presence of XanX at a concentration of 10 μg/mL and the MTT assay indicated that XanX was not cytotoxic to A549RT-eto cells at 10 μg/mL for 24 hours (Fig. 2B). When A549RT-eto cells were treated with XanX (10 μg/mL) at 12 hours after post-treatment, we found that XanX treatment reduced the expression levels of HDAC4, STAT1, p-STAT1, and P-gp (Fig. 2C) (***P < 0.001, XanX vs. control). The result indicates that XanX can suppress STAT1-HDAC4 signaling and

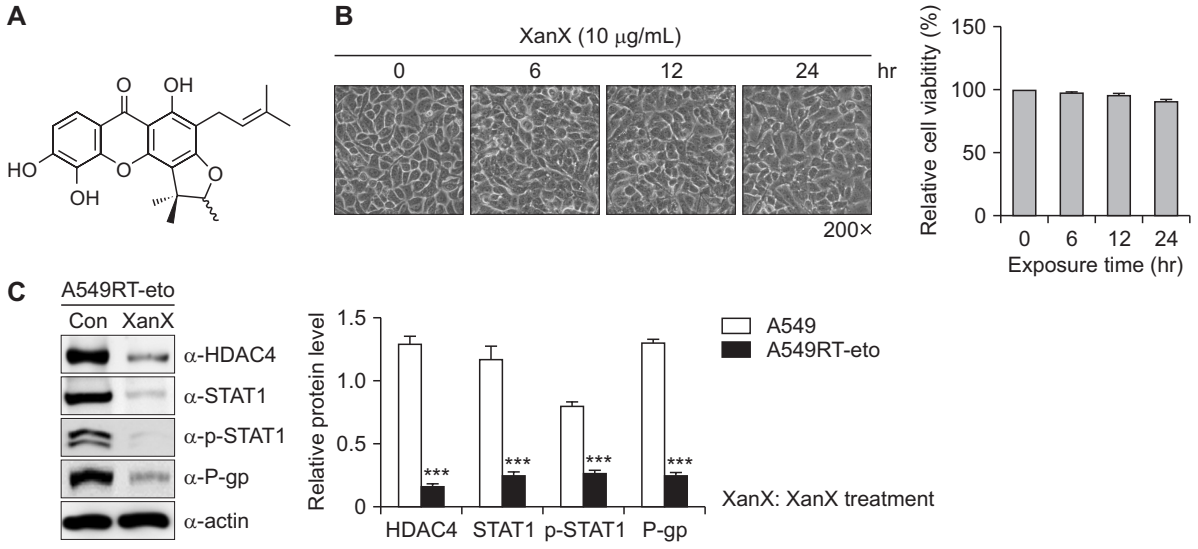

Figure 2. Cytotoxic and inhibitory effect of XanX on A549RT-eto cells and the expression of STAT1 and HDAC4. (A) Structure of XanX. (B) A549RT-eto cells were treated with XanX 10 μg/mL after treatment; the morphological changes of the cells were observed under a light microscope and cytotoxicity were measure by MTT assay after 0, 6, 12 and 24 hours. ×200 magnifications. (C) Cell lysates from A549RT-eto cells in the presence and absence of XanX (10 μg/mL) after 12 hours were prepared and separated on a 12% SDS-PAGE gel. The expressions of HDAC4, STAT1, p-STAT1 and P-gp protein were detected by immunoblotting with the corresponding antibodies. Densitometric analysis was performed on all blots done in triplicate and the integrated optical density of each band was normalized with corresponding β-actin (***P < 0.001, XanX vs. the control). XanX, formoxanthone C; A549RT-eto, A549 lung cancer cells resistant to etoposide; STAT1, signal transducer and activator of transcription 1; HDAC4, histone deacetylase 4; SDS, sodium dodecyl sulfate; PAGE, polyacrylamide gel electrophoresis; con, control; P-gp, P-glycoprotein; p-STAT1, phospho-signal transducer and activator of transcription 1.

reverse drug resistance by suppressing P-gp protein levels.

XanX inhibits EMT and stemness in A549RT-eto cells

Conventional chemotherapy usually shows inefficiency in eradicating CSC because CSC harbor some mechanisms for anti-cancer drug resistance [29]. Therefore, as it is a challenge to search for anticancer drugs to overcome these cancer cells bearing CSC-like phenotypes, we tested whether XanX can block CSC-like phenotypes in A549RT-eto cells. First, we performed wound-healing assays to evaluate the effects of XanX on the migration of A549RT-eto cells. For this purpose, the cells were incubated at a non-cytotoxic dose (10 μg/mL) of XanX for 24 hours. The results showed significantly decreased cell migration rates in A549RT-eto cells (Fig. 3A) (***P < 0.001, XanX vs. control). We also examined their cell invasion ability using a three-dimensional Matrigel-coated filter after A549RT-eto cells were treated with XanX. As

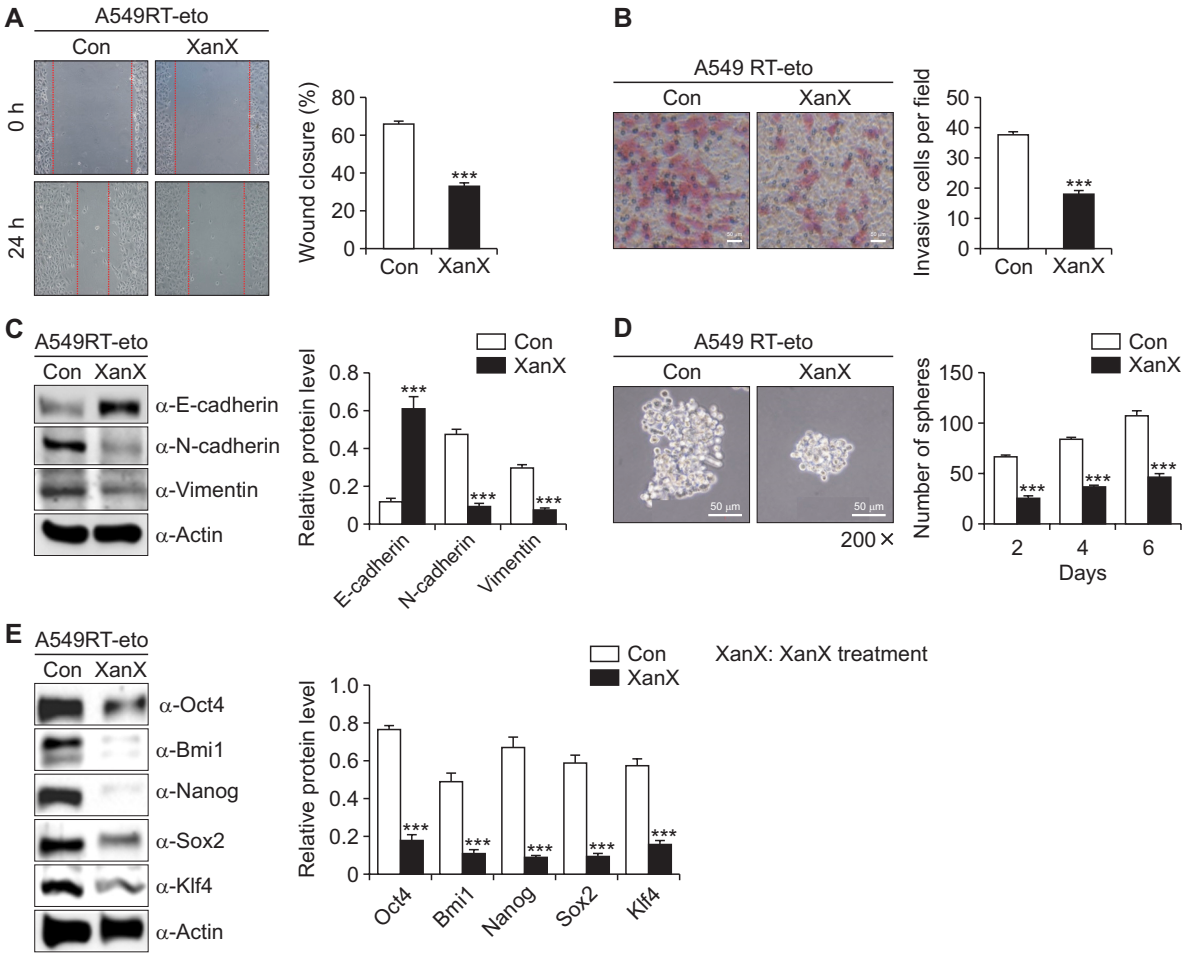

Figure 3. The effect of XanX on cell migration, invasion, and spheroid formation in A549RT-eto cells. (A) A549RT-eto cells were treated with XanX (10 μg/mL) for 24 hours, followed by the cell scratch assay performed to evaluate the migration ability of the treated cells (***P < 0.001 XanX vs. control). (B) A549RT-eto cells were treated as indicated, and a transwell assay was used to evaluate the effect of XanX on the invasion of the cells. The data are representative of three independent experiments and statistical analysis of the invading cells (***P < 0.001, XanX vs. control). An invasion assay was performed using 24-well chambers coated with Matrigel after 24 hours. The invading cells in the membrane were stained with hematoxylin-eosin (Magnification: ×200). (C) Cell lysates from A549RT-eto cells treated with XanX were prepared and separated on a 12% SDS-PAGE gel. The expressions of E-cadherin, N-cadherin, and vimentin proteins were detected by immunoblotting with the corresponding antibodies. Densitometric analysis was performed on all blots done and the integrated optical density of each band was normalized with corresponding β-actin (***P < 0.001, XanX vs. the control). ×200 magnifications. (D) A549RT-eto cells were treated with XanX (10 μg/mL) for 24 hours and were then plated and cultured in non-adherent 24-well flat-bottom plates for 6 days. Spheroid formation was observed at intervals over 48 hours (scale bars = 50 μm). The numbers of spheroids were counted on 2, 4 and 6 days. The data are representative of three independent experiments (***P < 0.001, XanX vs. control). (E) Cell lysates from A549RT-eto cells treated with XanX were prepared and separated on a 12% SDS-PAGE gel. The expressions of Oct4, Bmi1, Nanog, Sox2 and Klf4 proteins were detected by immunoblotting with the corresponding antibodies. Densitometric analysis was performed on all blots done and the integrated optical density of each band was normalized with corresponding β-actin (***P < 0.001, XanX vs. control). XanX, formoxanthone C; con, control; A549RT-eto, A549 lung cancer cells resistant to etoposide; con, control; SDS, sodium dodecyl sulfate; PAGE, polyacrylamide gel electrophoresis.

shown in Figure 3B, the treatment of A549RT-eto cells with XanX significantly decreased the cell invasion rates (approximately two-fold) compared to those of the cells that received the control treatment (***P < 0.001, XanX vs. control). Since XanX inhibited cell migration and invasion, we next examined the mechanism underlying its inhibition of EMT by measuring the levels of relevant protein markers. It is characterized by downregulation of E-cadherin and vimentin expression and upregulation of N-cadherin protein. We found that XanX treatment increased the expression of E-cadherin, whereas

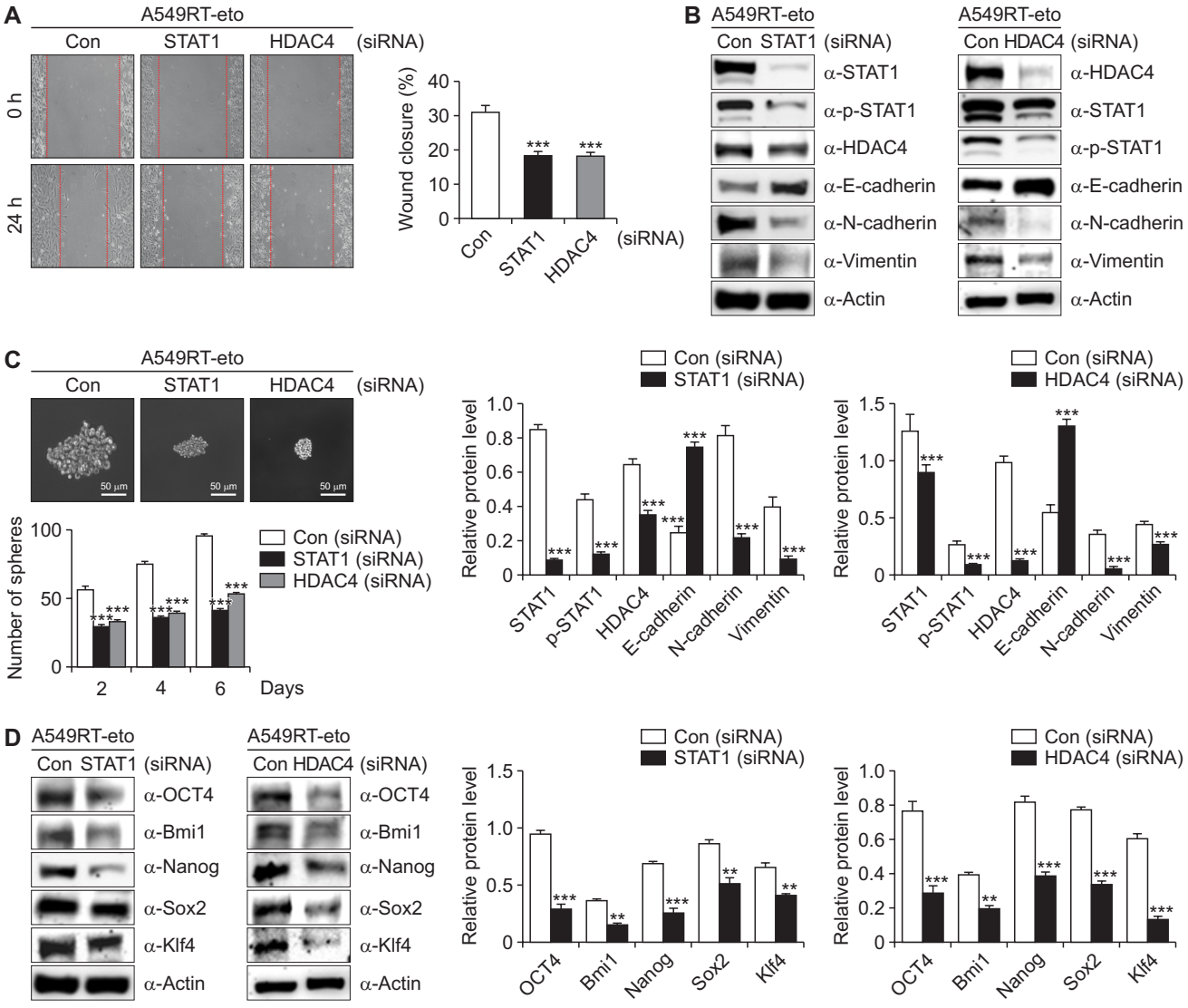

Figure 4. The effect of STAT1 or HDAC4 suppression on cell invasion and spheroid formation in A549RT-eto cells. (A) A549RT-eto cells were transfected with a control, STAT1 or HDAC4 siRNA (100 nM) and a transwell assay was used to evaluate the effect of STAT1-HDAC4 suppression on the invasion of the cells. The data are representative of three independent experiments (***P < 0.001, STAT1/HDAC4 vs. control siRNA). (B) Cell lysates from A549RT-eto cells treated with XanX were prepared and separated on a 12% SDS-PAGE gel. The expressions of E-cadherin, N-cadherin, vimentin, and STAT1, p-STAT1 and HDAC4 proteins were detected by immunoblotting with the corresponding antibodies. Densitometric analysis was performed on all blots done and the integrated optical density of each band was normalized with corresponding β-actin. (**P < 0.05 and ***P < 0.001, STAT1/HDAC4 vs. control siRNA) (C) The transfected cells were trypsinized and cultured in non-adherent 24-well flat-bottom plates for time-lapse recording for 6 days. Spheroid formation was observed at intervals over 48 hours (scale bars = 50 μm). The numbers of spheroids were counted for 6 days. The data are representative of three independent experiments (***P < 0.001, STAT1/HDAC4 compared to the control group). (D) The cell lysates from A549RT-eto cells treated with the control, STAT1 or HDAC4 siRNAs were prepared and separated on a 12% SDS-PAGE gel. The expressions of Oct4, Bmi1, Nanog, Klf4 and Sox2 proteins were detected by immunoblotting with the corresponding antibodies. Densitometric analysis was performed on all blots done and the integrated optical density of each band was normalized with corresponding β-actin (**P < 0.05 and ***P < 0.001, STAT1/ HDAC4 vs. control siRNA). STAT1, signal transducer and activator of transcription 1; HDAC4, histone deacetylase 4; A549RT-eto, A549 lung cancer cells resistant to etoposide; SDS, sodium dodecyl sulfate; PAGE, polyacrylamide gel electrophoresis; con, control; siRNA, small interfering RNA; p-STAT1, phospho-signal transducer and activator of transcription 1.

inhibited that of N-cadherin and vimentin proteins. Therefore, XanX can potentially inhibit that EMT by modulating the expression of E-cadherin, N-cadherin, and vimentin proteins (Fig. 3C) (***P < 0.001, XanX vs. control). In order to explore whether XanX inhibits stemness in vitro, we examined the effects of XanX treatment on sphere formation in A549RT-eto cells. As shown in Figure 3D, XanX treatment reduced the size and the number of spheroid formation compared to the control treatment (***P < 0.001, XanX vs. control). The expression of transcription factors or co-activators responsible for stemness such as Oct4, Bmi1, Sox2 and Klf4 was measured. As shown in Figure 3E, XanX treatment reduced the protein levels of Oct4, Bmi1, Sox2 and Klf4. These results suggest that XanX has the capability to inhibit CSC-like phenotypes in A549RT-eto cells (***P < 0.001, XanX vs. control).

STAT1-HDAC4 signaling is involved in the malignant tumor features of A549RT-eto cells

Since XanX treatment inhibited STAT1 and HDAC4 expression and activity as well as malignant tumor features (Fig. 2 and 3), a question arose as to whether STAT1-HDAC4 signaling is involved to silence expression of these malignant tumor features. Thus, siRNA was introduced to silence STAT1 and HDAC4. The treatment with STAT1 and HDAC4 siRNA inhibited migration of A549RT-eto cells (Fig. 4A) (***P < 0.001, STAT1/HDAC4 vs. control siRNA). In agreement this finding, STAT1-HDAC4 signaling increased the E-cadherin levels and decreased the N-cadherin and vimentin levels (Fig. 4B) (**P < 0.05 and ***P < 0.001, STAT1-HDAC4 vs. control siRNA). In addition, the knockdown of STAT1-HDAC4 diminished the spheroid size and the number of spheroids in A549RT-eto cells (Fig. 4C) (***P < 0.001, STAT1/HDAC4 compared to the control group). Moreover, the silencing of STAT1-HDAC4 led to a reduction in the protein levels of Oct4, Bmi1, Sox2 and Klf4 (Fig. 4D) (**P < 0.05 and ***P < 0.001, STAT1-HDAC4 vs. control siRNA). Therefore, STAT1-HDAC4 signaling was involved in manifestation of CSC-like phenotypes. Taken together, XanX treatment inhibited EMT and stemness through blockade of STAT1-HDAC4 signaling.

DISCUSSION

In our study, the levels of STAT1 and HDAC4 proteins were enhanced in A549RT-eto cells compared to those in the A549 parental cells [4]. Some studies have shown that activation of STAT1 and HDAC4 is associated with chemoresistance [4,19,30]. Thus, the suppression of STAT1 and HDAC inhibited manifestation of CSC-like phenotypes, including cell migration, invasion, and sphere formation in A549RT-eto cells. Our study further demonstrated that the decrease in STAT1 and HDAC4 levels by XanX treatment diminished the expression of mesenchymal protein markers such as N-cadherin and vimentin but enhanced the expression of the epithelial protein marker E-cadherin. The decrease in STAT1 and HDAC4 levels by XanX treatment also led to the reduced expression of stem cell transcription factors (Oct4, Bmi1, Nanog, Sox2 and Klf4) in A549RT-eto cells. The stemness-related transcription factors were found to be overexpressed in several cancers, including breast cancer, prostate cancer, and oral squamous cell carcinoma, and their expression levels are associated with malignant transformation, tumorigenicity, and tumor metastasis [31]. On the basis of these studies, we propose that the decrease in STAT1 and HDAC4 levels can be potential resolution of anticancer agents in treating other cancers in addition to A549 lung cancer with MDR. Therefore, STAT1-HDAC4 signaling becomes one of the most suitable candidates for therapeutic targets in the management of cancer [30]. This observation necessitates the exploration and development of anticancer agents targeting STAT1-HDAC4 signaling targeting ability.

Many approaches exploit the differences in cell surface markers to identify compounds that selectively target cancer cells. These targets include the ABC transporter superfamily, Wnt/β-catenin, TGF-β, Hedgehog, EGFR and Notch [32-34]. Recently, several compounds such as vitamins A and D, genistein, epigallocatechin gallate, sulforaphane, piperine, theanine, choline and curcumin have been shown to target malignant tumor features, particularly in combination with conventional chemotherapy drugs. They have been shown to significantly suppress self-renewal, induce differentiation, and inhibit tumor growth and metastasis [32]. Herein, we present novel finding that XanX treatment decreases the levels of P-gp through inhibition of STAT1-HDAC4 signaling. Downregulation of STAT1-HDAC4 signaling by XanX may be a key to solve some major obstacles in malignant cancer therapy, namely cancer relapse and chemotherapy resistance.

FUNDING

This study was supported by IPST for research funds for DPST graduate with first replacement (No.03/2557). The study was also supported by the Korea Institute for Advancement of Technology (KIAT) grant funded by Korea Government (MOTIE) (P0008763, The Competency Development Program for Industry Specialist; and N0002310, Construction Project of Supporting Center for Commercializing Customized Nano-mold-based Technologies).

CONFLICTS OF INTEREST

No potential conflicts of interest were disclosed.

ORCID

Chutima Kaewpiboon, https://orcid.org/0000-0003-2519-3796
Nawong Boonnak, https://orcid.org/0000-0002-6230-5438
Sirichat Kaowinn, https://orcid.org/0000-0002-5945-917X
Natpaphan Yawut, https://orcid.org/0000-0002-7201-6576

Young-Hwa Chung, https://orcid.org/0000-0001-5738-7400

REFERENCES

1. Song J, Ren W, Xu T, Zhang Y, Guo H, Zhu S, et al. Reversal of multidrug resistance in human lung cancer cells by delivery of 3-octadecylcarbamoylacrylic acid-cisplatin-based liposomes. Drug Des Devel Ther 2017;11:441-9.
2. Callaghan R, Luk F, Bebawy M. Inhibition of the multidrug resistance P-glycoprotein: time for a change of strategy? Drug Metab Dispos 2014;42:623-31.
3. Zhou P, Li B, Liu F, Zhang M, Wang Q, Liu Y, et al. The epithelial to mesenchymal transition (EMT) and cancer stem cells: implication for treatment resistance in pancreatic cancer. Mol Cancer 2017;16:52.
4. Kaewpiboon C, Srisuttee R, Malilas W, Moon J, Oh S, Jeong HG, et al. Upregulation of Stat1-HDAC4 confers resistance to etoposide through enhanced multidrug resistance 1 expression in human A549 lung cancer cells. Mol Med Rep 2015;11:2315-21.
5. Tanaka A, Zhou Y, Ogawa M, Shia J, Klimstra DS, Wang JY, et al. STAT1 as a potential prognosis marker for poor outcomes of early stage colorectal cancer with microsatellite instability. PLoS One 2020;15:e0229252.
6. Chin YE, Kitagawa M, Su WC, You ZH, Iwamoto Y, Fu XY. Cell growth arrest and induction of cyclin-dependent kinase inhibitor p21 WAF1/CIP1 mediated by STAT1. Science 1996;272:719-22.
7. Townsend PA, Scarabelli TM, Davidson SM, Knight RA, Latchman DS, Stephanou A. STAT-1 interacts with p53 to enhance DNA damage-induced apoptosis. J Biol Chem 2004;279:5811-20.
8. Stephanou A, Brar BK, Knight RA, Latchman DS. Opposing actions of STAT-1 and STAT-3 on the Bcl-2 and Bcl-x promoters. Cell Death Differ 2000;7:329-30.
9. Fryknäs M, Dhar S, Oberg F, Rickardson L, Rydåker M, Göransson H, et al. STAT1 signaling is associated with acquired crossresistance to doxorubicin and radiation in myeloma cell lines. Int J Cancer 2007;120:189-95.
10. Roberts D, Schick J, Conway S, Biade S, Laub PB, Stevenson JP, et al. Identification of genes associated with platinum drug sensitivity and resistance in human ovarian cancer cells. Br J Cancer 2005;92:1149-58.
11. Lo UG, Pong RC, Yang D, Gandee L, Hernandez E, Dang A, et al. IFNγ-induced IFIT5 promotes epithelial-to-mesenchymal transition in prostate cancer via miRNA processing. Cancer Res 2019;79:1098-112.
12. Qadir AS, Ceppi P, Brockway S, Law C, Mu L, Khodarev NN, et al. CD95/Fas increases stemness in cancer cells by inducing a STAT1-dependent type I interferon response. Cell Rep 2017;18:2373-86.
13. Yang XJ, Seto E. HATs and HDACs: from structure, function and regulation to novel strategies for therapy and prevention. Oncogene 2007;26:5310-8.
14. Geng H, Harvey CT, Pittsenbarger J, Liu Q, Beer TM, Xue C, et al. HDAC4 protein regulates HIF1α protein lysine acetylation and cancer cell response to hypoxia. J Biol Chem 2011;286:38095-102.
15. Mihaylova MM, Vasquez DS, Ravnskjaer K, Denechaud PD, Yu RT, Alvarez JG, et al. Class IIa histone deacetylases are hormone-activated regulators of FOXO and mammalian glucose homeostasis. Cell 2011;145:607-21.
16. Singh BN, Zhang G, Hwa YL, Li J, Dowdy SC, Jiang SW. Nonhistone protein acetylation as cancer therapy targets. Expert Rev Anticancer Ther 2010;10:935-54.
17. Zeng LS, Yang XZ, Wen YF, Mail SJ, Wang MH, Zhang MY, et al. Overexpressed HDAC4 is associated with poor survival and promotes tumor progression in esophageal carcinoma. Aging (Albany NY) 2016;8:1236-49.
18. Kaowinn S, Kaewpiboon C, Koh SS, Krämer OH, Chung YH. STAT1-HDAC4 signaling induces epithelial-mesenchymal transition and sphere formation of cancer cells overexpressing the oncogene, CUG2. Oncol Rep 2018;40:2619-27.
19. Kaowinn S, Jun SW, Kim CS, Shin DM, Hwang YH, Kim K, et al. Increased EGFR expression induced by a novel oncogene, CUG2, confers resistance to doxorubicin through Stat1-HDAC4 signaling. Cell Oncol (Dordr) 2017;40:549-61.
20. Cragg GM, Pezzuto JM. Natural products as a vital source for the discovery of cancer chemotherapeutic and chemopreventive agents. Med Princ Pract 2016;25(Suppl 2):41-59.
21. Boonnak N, Chantrapromma S, Fun HK. Molecular and crystal structures of α,α,β-Trimethylfuranylxanthone from *Cratoxylum formosum* ssp. *pruniflorum*: a partial racemate. Mol Cryst Liq Cryst 2015;606:165-75.
22. Kaewpiboon C, Boonnak N, Kaowinn S, Chung YH. Formoxanthone C, isolated from Cratoxylum formosum ssp. pruniflorum, reverses anticancer drug resistance by inducing both apoptosis and autophagy in human A549 lung cancer cells. Bioorg Med Chem Lett 2018;28:820-5.
23. Laphookhieo S, Maneerat W, Koysomboon S. Antimalarial and cytotoxic phenolic compounds from Cratoxylum maingayi and Cratoxylum cochinchinense. Molecules 2009;14:1389-95.
24. Kanintronkul Y, Worayuthakarn R, Thasana N, Winayanuwattikun P, Pattanapanyasat K, Surarit R, et al. Overcoming multidrug resistance in human lung cancer with novel benzo[a]quinolizin-4-ones. Anticancer Res 2011;31:921-7.
25. Kaewpiboon C, Surapinit S, Malilas W, Moon J, Phuwapraisirisan P, Tip-Pyang S, et al. Feroniellin A-induced autophagy causes apoptosis in multidrug-resistant human A549 lung cancer cells. Int J Oncol 2014;44:1233-42.
26. Leong SY, Ong BK, Chu JJ. The role of Misshapen NCK-related kinase (MINK), a novel Ste20 family kinase, in the IRES-mediated protein translation of human enterovirus 71. PLoS Pathog 2015;11:e1004686.
27. Phi LTH, Sari IN, Yang YG, Lee SH, Jun N, Kim KS, et al. Cancer stem cells (CSCs) in drug resistance and their therapeutic implications in cancer treatment. Stem Cells Int 2018;2018:5416923.
28. Mehta P, Novak C, Raghavan S, Ward M, Mehta G. Self-renewal

and CSCs in vitro enrichment: growth as floating spheres. Methods Mol Biol 2018;1692:61-75.
29. Shibue T, Weinberg RA. EMT, CSCs, and drug resistance: the mechanistic link and clinical implications. Nat Rev Clin Oncol 2017;14:611-29.
30. Stronach EA, Alfraidi A, Rama N, Datler C, Studd JB, Agarwal R, et al. HDAC4-regulated STAT1 activation mediates platinum resistance in ovarian cancer. Cancer Res 2011;71:4412-22.
31. Zakaria N, Mohd Yusoff N, Zakaria Z, Widera D, Yahaya BH. Inhibition of NF-κB signaling reduces the stemness characteristics of lung cancer stem cells. Front Oncol 2018;8:166.
32. Ahmed M, Chaudhari K, Babaei-Jadidi R, Dekker LV, Shams Nateri A. Concise review: emerging drugs targeting epithelial cancer stem-like cells. Stem Cells 2017;35:839-50.
33. Singh A, Settleman J. EMT, cancer stem cells and drug resistance: an emerging axis of evil in the war on cancer. Oncogene 2010;29:4741-51.
34. Giudice FS, Pinto DS Jr, Nör JE, Squarize CH, Castilho RM. Inhibition of histone deacetylase impacts cancer stem cells and induces epithelial-mesenchyme transition of head and neck cancer. PLoS One 2013;8:e58672.